

An Oracle Method to Couple Climate and Economic Dynamics

**L. Drouet, N. R. Edwards, C. Beltran, A. B. Haurie,
J.-P. Vial, and D. S. Zachary**

January, 2004



**Swiss National Centre of Competence (NCCR) "Climate"
Work Package 4: "Climate Risk Assessment"
University of Geneva & Paul Scherrer Institute**

Contact: Prof. Alain B. Haurie

University of Geneva

40, Bld du Pont d'Arve

CH-1211 Geneva, Switzerland.

Phone +41-22-705- 8132

Webpage: <http://ecolu-info.unige.ch/~nccrwp4/>

Copyright © *date* NCCR-WP4. All rights reserved.

No portion of this paper may be reproduced without permission of the authors

An Oracle Method to Couple Climate and Economic Dynamics*

Laurent Drouet[†] Neil R. Edwards[‡] Cesar Beltran[§] Alain B. Haurie[¶]
Jean-Philippe Vial^{||} Daniel S. Zachary^{**}

January 12, 2004

Abstract

This paper deals with an oracle method to couple economic and climate models. The approach permits a dialogue between two models pertaining to two different scientific domains, the climate module being a fully-coupled ocean-atmosphere-sea ice model, whereas the economic module is an adaptation of the neo-classical optimal economic growth paradigm. The paper explains how the Analytic Centre Cutting Plane Method (ACCPM) is implemented to integrate in the optimal economic growth model a constraint on climate change that is computed from the climate model runs. Several experiments show the usefulness of the approach to build new types of integrated assessment meta-models

1 Introduction

The aim of this paper is to describe an oracle method that is used to couple an economic growth model, namely an adaptation of the DICE99 model of Nordhaus [26], with an efficient climate model with three-dimensional ocean dynamics, in our case C-GOLDSTEIN [8]. The coupling is implemented through the use of a large-scale convex programming method, called ACCPM¹ [12]. In this approach, a dialogue is established between the economic model and the climate model through the exchange of a coupling vector of variables, namely the schedule of atmospheric concentration of GHGs over a series of milestones encompassing a 200 year planning horizon. The two models play the role of “oracles” which respond to a proposed concentration schedule with an economic growth scenario and a distribution of temperature increases respectively. In ACCPM, a master program controls this exchange of information between the two models in order to obtain an optimal economic growth that satisfies a climate impact constraint represented by a bound on an “area over threshold” (AOT) temperature functional. This method has already been successfully used to couple a techno-economic energy model and a local air pollution (ozone) model, as reported in [5]. The advantage of the method is that it permits the analyst to retain each model in its full generality and level of detail and to overcome the difficulties tied with the different time and space scales involved in economics and climate models respectively. This

*This work has been supported by the SNSF-NCCR “Climate” grant.

[†]Logilab-HEC, University of Geneva, Switzerland.

[‡]Climate and Environmental Physics,, University of Bern, Switzerland.

[§]Logilab-HEC, University of Geneva, Switzerland.

[¶]Logilab-HEC, University of Geneva, Switzerland.

^{||}Logilab-HEC, University of Geneva, Switzerland.

^{**}Physics Department, American University of Sharjah, Sharjah (U.A.E.), University of Geneva, Switzerland

¹Analytic Center Cutting Plane Method.

approach is similar in spirit to the *Community integrated assessment* advocated in [18] for coupling insights gained from different modelling communities.

The paper is organized as follows: in section 2 we discuss the challenge of developing integrated assessment models for climate policies in which economic, climate and impact submodels have to be linked together in a coherent whole; in section 3 we briefly describe the main features of the C-GOLDSTEIN model; in section 4 we present an adaptation of the DICE99 model where the equations representing temperature increase and impacts have been removed; in section 5 we describe the implementation of ACCPM to realize the coupling; in section 6 we present numerical results for a set of simulations and in Conclusion we envision other possible implementations of the method and we discuss its usefulness for the creation of a new class of integrated assessment meta-models.

2 The challenge of integrated assessment

DICE94 [24, 25] and IMAGE [2] are the archetypal integrated assessment models² for climate change policies. In the case of DICE94, a neo-classical economic growth model has been augmented to include simplified representations of the accumulation of GHGs and of the resulting increase in average atmospheric temperature, as well as the economic impact (represented as a production loss) of this temperature change. In the case of IMAGE the model contains representations of three major subsystems, namely climate, biosphere and society. The global model components corresponding to these subsystems describe the atmosphere and ocean, the terrestrial environment and the energy and industry. Several other IAMs have been proposed recently. We shall refer in particular to DICE99 and RICE that are the successors of DICE94 with an improved description of the carbon cycle and a multi-regional description of the economic growth process, and to ICLIPS [1] that has been developed and used for the definition of *tolerable windows* in climate change scenarios. Another strand of IAM development is represented by the MERGE model [22] based on a combination of a macro-economic growth, an energy use and a temperature change sub-model.

In all these examples of IAMs the modellers have created a single system that integrates the descriptions of the different sub-systems in modules that are interconnected. In doing this integration the model developers have had to solve delicate problems of time and space scaling in the joint representation of the dynamics in different submodules. Typically in IAMs the description of the temperature change dynamics is reduced to a very schematic form, compared to the description used in GCMs. In such a representation the IAM remains highly computationally efficient, the simple form of the climate representation allowing optimal solutions to be obtained,

²We quote below the definition proposed in the Ulysses project web site
<http://www.zit.tu-darmstadt.de/ulysses>

Integrated Assessment (IA) can be defined as an interdisciplinary process of combining, interpreting and communicating knowledge from diverse scientific disciplines in such a way that the whole cause-effect chain of a problem can be evaluated from a synoptic perspective with two characteristics: (i) it should have added value compared to single disciplinary assessment; and (ii) it should provide useful information to decision makers.

Integrated Assessment Model (IAM) : a computer simulation program representing a coupled natural system and a socio-economic system, modelling one or more cause-effect chains including feedback loops, and explicitly designed to serve as a tool to analyse policies in order to guide and inform the policy process, mostly by means of scenario analysis. This explicit policy purpose defines the difference between IAMs and Earth System Models (ESMs) such as Atmosphere Ocean General Circulation Models (GCMs) and geochemical models, which are designed primarily for scientific purposes. It should however be noted that ESMs such as GCMs could also be used (and in fact they are) to look at policy questions.

often by relying on the analytical form of the representation to invert the relation between climate forcing and climatic response. In contrast, the models most widely used in the climate modelling community to predict possible climatic responses to anthropogenic forcing, have high spatial resolution and can take months of computation to simulate a few hundred years, while the dynamics of the system are such that the full impact of the forcing is only realised on a timescale of thousands of years. Furthermore, each integration of such a model is only a single realisation of a chaotic system. The analysis of the expected feedback between policy choices and climatic responses, and the associated uncertainties, in a coupled IAM would clearly be exceptionally difficult using such climate models. However, simpler climate models are severely restricted in their ability to faithfully represent dynamical responses and regional contrasts.

Taking a step towards the use of more complex climate modules in IAMs [3] use the reduced dimensionality Bern 2.5D model to estimate constraints on total atmospheric warming and rate of warming to avoid a collapse of the Atlantic thermohaline circulation (THC). These constraints are then applied to the extremely simple, analytical climate submodule within MERGE. In this approach MERGE is therefore able to make use of results from a somewhat more realistic climate model although not in a fully consistent way. In this paper we demonstrate the possibility of incorporating a climate model, in our case with a fully 3-dimensional ocean component, within the solution procedure of the IAM. Thus the climatic response to forcing assumed by the economic module is consistently produced by the climate module itself at every iteration. Our approach is still not completely consistent, since the climate module does not include a complete, closed carbon cycle, thus the transfer of atmospheric carbon to the surface and deep ocean is still represented by the simple, 3-equation system of DICE99. However, this inconsistency could be removed by the inclusion of the appropriate climatic processes without modification to the fundamental structure of our integrated modelling approach. The present system, although simplified, is therefore sufficient to demonstrate the effectiveness of the coupling strategy itself. In a subsequent paper we plan to repeat the experiment, directly simulating the ocean and land carbon cycle using the coupled Earth System Model developed in the GENIE (Grid Enabled Integrated Earth System Model) project [11], which includes C-GOLDSTEIN as a subcomponent.

3 The climate model: C-GOLDSTEIN

We use a simplified climate model, C-GOLDSTEIN, which is intermediate in complexity and computational efficiency between the intensively studied and very costly general circulation models (GCMs) such as HadCM3 [15] or CCSM [4], and highly efficient models of lower dimensionality such as the Bern 2.5-D model. The latter uses 2-D representations of the flow in each ocean basin following [35], whereas C-GOLDSTEIN has low resolution, but includes a fully 3-D global ocean, coupled to a 2-D atmosphere and a dynamical and thermodynamical sea-ice component. Largely as a result of low resolution and simplified dynamics, the model is significantly more efficient than other intermediate complexity climate models described in the literature, such as the UVic model [34], FORTE [31] and ECBILT-CLIO [14], taking one or two hours to complete a 1000-year integration on a PC. The model is described in detail by [8] who show that it gives a reasonable representation of modern climate and also investigate the model's parameter sensitivity using an ensemble of 1000 runs of 2000 years in length. Using the same model, [23] consider the possibility of a collapse of the North Atlantic thermohaline circulation in an extensive study representing around 40 million years of total integration time. It is thus an appropriately simple and efficient model, capable of representing at least some of the expected large-scale climatic responses to anthropogenically induced climate change. Below we give a concise summary of the dynamics of each model subcomponent.

3.1 Ocean component

The ocean model is based on the thermocline (or planetary geostrophic) equations with the addition of a linear drag term in the horizontal momentum equations. We therefore refer to the model as a frictional geostrophic (FG) model. Dynamically, the model is therefore similar to classical GCMs, but neglects momentum advection and acceleration. The ocean density, ρ , depends nonlinearly on the local values of temperature T and salinity S , which obey separate advection-diffusion equations and are also subject to convective adjustment. Earlier versions of the model were used by [10], [9], [7].

Referred to spherical polar coordinates (ϕ, s, z) , where ϕ is longitude, $s = \sin\theta$, θ is latitude and z is measured vertically upwards, the governing equations can be expressed in the dimensionless form

$$-sv = -\frac{1}{c} \frac{\partial p}{\partial \phi} - \lambda u, \quad (1)$$

$$su = -c \frac{\partial p}{\partial s} - \lambda v, \quad (2)$$

$$\frac{\partial p}{\partial z} = -\rho, \quad (3)$$

$$\frac{\partial}{\partial \phi} \left(\frac{u}{c} \right) + \frac{\partial}{\partial s} (vc) + \frac{\partial w}{\partial z} = 0, \quad (4)$$

$$\rho = \rho(S, T), \quad (5)$$

$$\frac{D}{Dt} X = \kappa_h \nabla^2 X + \frac{\partial}{\partial z} \left(\kappa_v \frac{\partial X}{\partial z} \right) + \mathcal{C}. \quad (6)$$

The horizontal momentum equations, (1) and (2), express the “geostrophic balance” between the Coriolis term on the left hand side and the gradient of perturbation pressure p , on the right, with the addition of a drag term with coefficient λ . The coefficient $c = \cos\theta$. Horizontal lengths have been scaled by the Earth’s radius r_0 ; vertical lengths by a typical mid-ocean depth H ; the horizontal velocity components (u, v) in the (ϕ, s) directions have been scaled by a typical horizontal velocity U ; and the vertical velocity w has been scaled by UH/r_0 . The vertical pressure gradient in Eq. (3) is in “hydrostatic balance” with the gravitational force. Scalings for p and density ρ are derived from the geostrophic and hydrostatic relations respectively. Eq. (4) expresses mass conservation and Eq. (6) the advection and diffusion of a tracer X representing temperature T or salinity S . D/Dt is the total (or material) derivative³. Scalings for S and T are not necessary because they appear linearly in equation (6); their magnitudes depend on the boundary forcing. The advective time scale r_0/U is used. In practice the horizontal and vertical diffusion of ocean tracers, represented by the second and third terms in Eq. (6), is replaced by an isopycnal diffusion and eddy-induced advection parameterisation in which a considerable simplification is obtained by setting the isoneutral diffusivity equal to the skew diffusivity representing eddy-induced advection, as suggested by Griffies [16]. \mathcal{C} is the convective adjustment term, which acts to remove gravitational instability while conserving S and T . The equation of state, Eq. (5), is linear in salinity S and cubic in temperature T . At all boundaries, the normal component of velocity is set to zero. The ocean is forced by fluxes of heat and salt through the upper boundary and by wind forcing, which is included as a source term in Eqs. (1) and (2) in the uppermost grid level. The fluxes of heat and salt through the lateral and lower boundaries are set to zero. A further modification to the ocean model is the inclusion of a variable upstream weighting for advection.

³ $D/Dt = \partial/\partial t + \mathbf{u} \cdot \nabla$ where $\mathbf{u} = (u, v, w)$ is the three-dimensional velocity vector.

The equations are discretized on an Arakawa ‘C’ grid using simple, second order, centred differences in space. A simple forward difference in time provides adequate accuracy, since the time step is limited by numerical constraints, and is twice as efficient as a centred difference in time, since the allowed time step is longer. At each time step the velocity field is determined diagnostically from the density field, and then relaxed back to the velocity used at the previous timestep. The barotropic (or depth-averaged) component of the flow is obtained by direct inversion of the elliptic equation resulting from the vertical integral of the momentum equations. Additionally, a set of linear constraints applies to the barotropic flow around islands. In the vertical there are normally 8 density levels on a uniformly logarithmically stretched grid with vertical spacing increasing with depth from 175 m to 1420 m. The maximum depth is set to 5 km. The horizontal grid is uniform in the (ϕ, s) , longitude $\sin(\text{latitude})$ coordinates giving boxes of equal area in physical space. The horizontal resolution is normally 36 by 36 cells.

3.2 Atmosphere and land surface

We use an Energy and Moisture Balance Model (EMBM) of the atmosphere, similar to that described in [34]. The prognostic variables are surface air temperature T_a and surface specific humidity q for which the governing equations can be written

$$\rho_a h_t C_{pa} \left(\frac{\partial T_a}{\partial t} + \nabla \cdot (\beta_T \mathbf{u} T_a) - \nabla \cdot (\kappa_T \nabla T_a) \right) = Q_{SW} C_A + Q_{LW} - Q_{PLW} + Q_{SH} + Q_{LH}, \quad (7)$$

$$\rho_a h_q \left(\frac{\partial q}{\partial t} + \nabla \cdot (\beta_q \mathbf{u} q) - \nabla \cdot (\kappa_q \nabla q) \right) = \rho_o (E - P) \quad (8)$$

where h_t and h_q are constant atmospheric boundary layer depths for heat and moisture respectively, κ_T and κ_q are eddy diffusivities for heat and moisture respectively, E is the evaporation or sublimation rate, P is the precipitation rate, ρ_a is air density, and ρ_o is a constant reference density of water. C_{pa} is the specific heat of air at constant pressure. The parameters β_T, β_q allow for a linear scaling of the advective transport term. This may be necessary as a result of the overly simplistic, one-layer representation of the atmosphere, particularly if surface velocity data are used in place of vertically averaged data, as in our standard runs. The values $\beta_T = 0, \beta_q = 0.4$ or 0 are used in [34]. We allow $\beta_T \neq 0$ but only for zonal advection, while β_q takes the same value for zonal and meridional advection. In view of the convergence of the grid, winds in the two gridpoints nearest each pole are averaged zonally to give smoother results in these regions.

In contrast to [34], the short-wave solar radiative forcing is temporally constant, representing annually averaged conditions. In a further departure from that model, the relevant planetary albedo is given by a simple cosine function of latitude. Over sea ice the albedo is temperature-dependent. The constant C_A parameterizes heat absorption by water vapour, dust, ozone, clouds, etc. The diffusivity κ_T , in our case, is given by a simple Gaussian function centred on the equator with specified magnitude, north-south slope and width. κ_q is spatially constant.

The remaining heat sources and sinks are as given in [34]: Q_{LW} is the long-wave imbalance at the surface; Q_{PLW} , the planetary long-wave radiation to space, is given by the polynomial function derived from observations by Thompson and Warren [33], cubic in temperature T_a and quadratic in relative humidity $r = q/q_s$ where q_s is the saturation specific humidity, which is exponential in the surface temperature. For anthropogenically forced experiments a greenhouse warming term is added which is proportional to the log of the relative increase in carbon dioxide (CO_2) concentration C as compared to an arbitrary reference value C_0 .

The sensible heat flux Q_{SH} depends on the air-surface temperature difference and the surface wind speed (derived from the ocean wind-stress data) and the latent heat release Q_{LH} is proportional to the precipitation rate P , as in [34]. In a departure from that model, however,

precipitated moisture is removed instantaneously, as in standard oceanic convection routines, so that the relative humidity r never exceeds its threshold value r_{\max} . This has significant implications as it means that the relative humidity is always equal to r_{\max} wherever precipitation is non-zero, effectively giving q the character of a diagnostic parameter. Here, since the model is used to represent very long-term average states, regions of zero precipitation only exist as a result of oversimplified representation of surface processes on large landmasses.

To improve efficiency we use an implicit scheme to integrate the atmospheric dynamical equations (7) and (8). The scheme comprises an iterative, semi-implicit predictor step [32] followed by a corrector step which renders the scheme exactly conservative. Changes per timestep are typically small, thus a small number of iterations of the predictor provides adequate convergence.

The model has no dynamical land surface scheme. The land surface temperature is assumed to equal the atmospheric temperature T_a , and evaporation is set to zero, thus the atmospheric heat source is simplified over land as the terms $Q_{LW} = Q_{SH} = Q_{LH} = 0$. Precipitation over land is added to appropriate coastal ocean gridcells according to a prescribed runoff map.

3.3 Sea ice and the coupling of model components

The fraction of the ocean surface covered by sea ice in any given region is denoted by A . Dynamical equations are solved for A and for the average height H of sea ice. In addition a diagnostic equation is solved for the surface temperature T_i of the ice. Following Semtner [30] and Hibler [17] thermodynamic growth or decay of sea ice in the model depends on the net heat flux into the ice from the ocean and atmosphere. Sea-ice dynamics simply consist of advection by surface currents and Laplacian diffusion with constant coefficient κ_{hi} .

The sea-ice module acts as a coupling module between ocean and atmosphere and great care is taken to ensure an exact conservation of heat and fresh water between the three components. The resulting scheme differs from the more complicated scheme of [34] and is described fully by [8].

Coupling is asynchronous in that the single timestep used for the ocean, sea-ice and surface flux calculation can be an integer multiple of the atmospheric timestep. Typically we use an atmospheric timestep of around a day and an ocean/sea-ice timestep of a few days. The fluxes between components are all calculated at the same notional instant to guarantee conservation, but are formulated in terms of values at the previous timestep, thus avoiding the complications of implicit coupling. All components share the same finite-difference grid.

3.4 Topography and runoff catchment areas

The seafloor topography is based on a Fourier-filtered interpolation of ETOPO5 observationally derived data. A consequence of the rigid-lid ocean formulation is that there is no mechanism for equilibration of salinity in enclosed seas which must therefore be ignored or connected to the ocean. In our basic topography the depth of the Bering Strait is a single level (175 m), thus it is open only to barotropic flow, which we usually ignore, and diffusive transport, while the Gibraltar Strait is two cells deep and thus permits baroclinic exchange flow.

Equivalently filtered data over land were used - along with depictions of major drainage basins in [34] and the Atlantic/Indo-Pacific runoff catchment divide of [36] - to guide the subjective construction of a simple runoff mask.

3.5 Freshwater flux redistribution

The single-layer atmosphere described above generates only around 0.03 Sv moisture transfer from the Atlantic to the Pacific (1 Sv = $10^6 \text{ m}^2\text{s}^{-1}$), whereas Oort [27] estimated a value of 0.32 Sv from observations. This typically leads to very weak deep sinking in the north Atlantic in

the model unless the moisture flux from the Atlantic to the Pacific is artificially boosted by a constant additional redistribution of surface freshwater flux. Following Oort, we transfer fresh water at a net rate F_a , subdivided into three latitude bands in the proportions found by Oort. Many ocean and climate models, including HadCM3 and the UVic model, artificially alter the geometry of the Denmark Strait to achieve the same effect on Atlantic deep sinking. An advantage of the approach used here is that the parameter F_a can easily be adjusted for sensitivity studies in altered climate states [23]. Note that our adjustment of surface freshwater fluxes is a pure redistribution and serves a quite different purpose from the flux adjustments used in early coupled climate models to prevent climate drift. Climate drift in higher-resolution models typically arises because the models are too costly to integrate to equilibrium. An important advantage of efficient climate models is that they do not suffer from this particular problem.

3.6 Default parameters and forcing fields

In principle, values used for oceanic isopycnal and diapycnal diffusivities, κ_h and κ_v and possibly momentum drag (Rayleigh friction) coefficient λ may need to be larger at low than at high resolution to represent a range of unresolved transport processes. In FG dynamics, the wind-driven component of the circulation tends to be unrealistically weak for moderate or large values of the frictional drag parameter λ , for reasons discussed in [21], while for low drag unrealistically strong flows appear close to the equator and topographic features. This problem is alleviated by allowing the drag λ to be variable in space. By default, drag increases by a factor of three at each of the two gridpoints nearest the equator or to an upper-level topographic feature. In addition, we introduce a constant scaling factor W which multiplies the observed wind stresses in order to obtain stronger and more realistic wind-driven gyres. For $1 < W < 3$ it is possible to obtain a wind-driven circulation with a reasonable pattern and amplitude. Annual mean wind-stress data for ocean forcing come from the the SOC climatology [19]. Wind fields used for atmospheric advection are long-term (1948 to 2002) annually averaged 10 m wind data derived from NCEP/NCAR reanalysis. Default parameters are given in Table 1.

3.7 Climate change assessment

To simulate the response to GHG forcing, we first need a quasi-steady initial condition representing the pre-industrial climate, which we obtain by integrating from a uniform state of rest with constant solar forcing for a period of 5600 years. We then integrate forwards in time using observed CO_2 concentrations from 1795 to 1995. The resulting state is then used as an initial condition for the fully coupled integrations in which the CO_2 concentrations are supplied by the economic growth model (the RCEG model to be introduced in Section 4). The origin on the time axis is henceforth taken to correspond to this initial condition at 1995.

The climate model supplies to the economic growth model a measure of climate change in the form of a set of criteria defined as scalar functionals of the trajectories of the climate state variables, for example atmospheric temperature T_a and humidity q , sea-ice area A or ocean temperature T and velocity \mathbf{u} . Later we experiment with several alternative criteria, but by default we use an Area Over Threshold (AOT) criterion for the globally averaged surface air temperature

$$D_{0,\theta} = \frac{\int_{\Omega} \mathbb{I}[T_a(\omega, 200) \geq \theta] d\omega}{\int_{\Omega} d\omega}, \quad (9)$$

where $T_a(\omega, 200)$ is the surface air temperature at location ω at horizon 200 years, Ω is the global domain, $\mathbb{I}[\cdot]$ is the indicator function and θ is a critical temperature rise. Another possible

Table 1: Default values of parameters for the climate model. The value given for λ is the minimum value in the ocean interior, while the value for κ_T is the maximum value at the equator. The full specification of variable drag, ocean density, isoneutral and eddy-induced mixing, surface fluxes, outgoing longwave radiation, specific humidity and freezing temperature involves a total of about 75 parameters, details of which are given or referred to by [8].

parameter	notation	value
ocean		
isopycnal diffusivity	κ_h	$2000 \text{ m}^2 \text{ s}^{-1}$
diapycnal diffusivity	κ_v	$1 \times 10^{-5} \text{ m}^2 \text{ s}^{-1}$
friction	λ	$1/2.5 \text{ days}^{-1}$
wind-scale	W	2
density	ρ_o	1000 kg m^{-3}
atmosphere		
T diffusivity amp.	κ_T	$8 \times 10^6 \text{ m}^2 \text{ s}^{-1}$
q diffusivity	κ_q	$8 \times 10^4 \text{ m}^2 \text{ s}^{-1}$
T advection coeff.	β_T	0.1
q advection coeff.	β_q	0.25
FWF adjust.	F_a	0.32 Sv (1 Sv= $10^6 \text{ m}^2\text{s}^{-1}$)
heat absorption	C_A	0.3
boundary layer depth (T)	h_t	8400 m
boundary layer depth (q)	h_q	1800 m
density	ρ_a	1.25 kg m^{-3}
specific heat capacity	C_{pa}	$1004 \text{ J kg}^{-1} \text{ K}^{-1}$
threshold relative humidity	r_{\max}	0.85
sea ice		
sea-ice diffusivity	κ_{hi}	$2000 \text{ m}^2 \text{ s}^{-1}$

criterion is the weighted AOT (WAOT) defined as follows

$$D_{\alpha(\cdot),\theta} = \frac{\int_{\Omega} \alpha(\omega) \mathbb{I}[T_a(\omega, 200) \geq \theta] d\omega}{\int_{\Omega} \alpha(\omega) d\omega}, \quad (10)$$

where $\alpha(\omega) \geq 0$ is a weighting function.

4 The economic model: RCEG

In this section we propose an aggregate economic growth model that represents the fundamental world economic dynamics, in the form of a control system where investment and emissions abatement are the control variables whereas capital stock and GHG concentrations, nominally in atmosphere, shallow and deep ocean, are the state variables, respectively. We use a reduced version of the DICE99 model which represents the economic growth process as a Ramsey model [29], [25], [26]; for this reason we name our model RCEG for *Ramsey-Concentration-and-Economic-Growth*. In simple terms and continuous time⁴ the model we use can be summarized as follows.

The state and control (policy) variables, the exogenous dynamic variables and the auxiliary variables that serve to define the reward function and the state equations are given in Table 2.

Table 2: List of variables in the RCEG model

List of endogenous state variables	
$K(t)$	= capital stock
$MA(t)$	= mass of GHG in the atmosphere (b.t.c.)
$MU(t)$	= mass of GHG in shallow oceans (b.t.c.)
$ML(t)$	= mass of GHG in lower oceans (b.t.c.)
List of control variables	
$I(t)$	= gross investment
$\mu(t)$	= rate of GHG emissions reduction
List of exogenous dynamic variables	
$A(t)$	= level of technology
$L(t)$	= labour input (=population)
$O(t)$	= forcing exogenous GHG
List of auxiliary variables	
$C(t)$	= total consumption
$c(t)$	= per capita consumption
$D(t)$	= damage from GH warming
$E(t)$	= emissions of GHGs
$ET(t)$	= emissions due to deforestation
$Q(t)$	= gross world product

⁴We prefer to use a continuous time control formalism to represent the economic growth model, although we shall use a discrete time version in the numerical experiments.

The equations of the model are listed below. The equations have been regrouped in different sets that will help to explain the structure of this economic model.

G1 – utility criterion

$$\max \int_0^{\infty} e^{-\rho t} U(c(t), L(t)) dt \quad (11)$$

$$U(c(t), L(t)) = L(t) \frac{c(t)^{1-\alpha} - 1}{1-\alpha} \quad (12)$$

G2 – exogenous population, technical progress, deforestation growth

$$\dot{L}(t) = g_L(t)L(t) \quad (13)$$

$$\dot{g}_L(t) = -\delta_L g_L(t) \quad (14)$$

$$\dot{A}(t) = g_A(t)A(t) \quad (15)$$

$$\dot{g}_A(t) = -\delta_A g_A(t) \quad (16)$$

$$ET(t) = ET(0)e^{-\delta_T t} \quad (17)$$

G3 – production and emissions

$$Q(t) = (1 - b_1 \mu(t)^{b_2}) A(t) K(t)^\gamma L(t)^{1-\gamma} \quad (18)$$

$$E(t) = (1 - \mu(t)) \sigma(t) Q(t) + ET(t) \quad (19)$$

G4 – Production usage

$$Q(t) = C(t) + I(t) \quad (20)$$

$$c(t) = \frac{C(t)}{L(t)} \quad (21)$$

G5 – capital accumulation

$$\dot{K}(t) = I(t) - \delta K(t) \quad (22)$$

G6 – GHG accumulation

$$\dot{\widehat{MA}}(t) = E(t) - \delta_{MAA}(MA(t)) + \delta_{MAU}(MU(t)) \quad (23)$$

$$\dot{\widehat{ML}}(t) = -\delta_{MLL}(ML(t)) + \delta_{MLU}(MU(t)) \quad (24)$$

$$\dot{\widehat{MU}}(t) = -\delta_{MUU}(MU(t)) + \delta_{MUA}(MA(t)) + \delta_{MUL}(ML(t)) \quad (25)$$

G7 – bounds on GHG concentrations

$$MA(t_i) \leq MA_i^{\text{sup}}; \quad i = 1, \dots, k \quad (26)$$

$$MA(t) \leq MA_i^{\text{sup}}; \quad t \geq t_k. \quad (27)$$

Eqs. (11)-(12) in group G1 describe the utility accumulation process. When $\alpha = 1$ the utility function takes the form $L \log(c)$. A key parameter is the discount rate ρ which is here geometrically decreasing over time; utility is derived from consumption by a growing population.

Eqs. (13)-(17) in group G2 describe the dynamics of some exogenously defined processes. They are the population growth, the technical progress and the deforestation processes, respectively. One notices that the population growth and the technical progress will tend to stabilize and the deforestation will also tend to disappear in the long run.

Eqs. (18)-(19) in group G3 describe the output and emissions processes. Output is the result of two production factors, labour L and capital K ; the abatement effort μ has a cost expressed as a loss of production. Emissions are a function of the carbon intensity of the production

technologies (parameter σ), and are reduced by the abatement effort μ . Exogenous emissions ET are due to deforestation.

Eqs. (20)-(21) in group G4 show that the output can be consumed or invested. Per-capita consumption is obtained from gross consumption and population level.

Eq. (22) in group G5 describes the capital accumulation process. The parameter δ is the depreciation rate of capital.

Eqs. (23)-(25) in group G6 describe the carbon accumulation process in a three-reservoir system, composed of atmosphere, shallow and deep ocean respectively. While it would be a relatively simple matter to replace these equations by directly simulating the transfer of carbon to the deep ocean within the climate model, we have not done so in this initial investigation.

Finally, Eqs. (26)-(27) in group G7 describe the bounds that will be imposed on the atmospheric concentrations of GHGs at some predetermined milestones (dates t_i , $i = 1, \dots, k$) and after time t_k . These constraints will be the linking variables with the climate model.

The parameter values are indicated below, in the units proposed by Nordhaus and Boyer.

Table 3: Parameter values

α	=	1
b_1	=	0.045
b_2	=	2.15
β	=	0.64
γ	=	0.25
δ_K	=	0.10 (per year)
δ_T	=	0.01 (per year)
δ_{MAA}	=	0.33384 (per decade)
δ_{MAU}	=	0.27607 (per decade)
δ_{MUU}	=	0.39103 (per decade)
δ_{MUA}	=	0.33384 (per decade)
δ_{MUL}	=	0.422 (per decade)
δ_{MLL}	=	0.0422 (per decade)
δ_{MLU}	=	0.1149 (per decade)
λ	=	1.41
θ_1	=	0.0007
θ_2	=	3.57
σ	=	0.033

In comparison with DICE99, the new control problem (11)-(27) defining the RCEG model no longer contains the equations which deal with temperature and forcing. The equation (18) was also modified as the production loss due to temperature impact is removed from the production function. We now run the model in a cost-effectiveness manner instead of the cost-benefit approach implemented by Nordhaus. For that purpose we introduce upper bounds on atmospheric concentrations (26)-(27) at milestones distributed 50 years apart along the time axis. The objective is to maximize the total welfare of the economic system subject to the concentration limits.

In our calculations we used a discrete-time version of the model, written in the GAMS modelling language, with time steps representing 10 years. This version will be used for numerical implementation.

5 The reduced order problem

We denote by $x = (MA_1^{\text{sup}}, \dots, MA_k^{\text{sup}})'$ the vector of upper bounds on GHG concentration limits at milestones t_i ($i = 1, \dots, k$), that will serve as the coupling variables between the economic and the climate models (technically we make a conversion here from mass to concentration). Normally $k = 4$ and $t_i = i \times 50$ years. In the climate model the values x_i are taken as actual concentrations at times t_i . The concentration at intermediate times $MA(t)$, also denoted as $x(t)$, is defined by linear interpolation. We call $V(x)$ the optimum value given by the solution of the control problem (11)-(27), when the concentration upper bounds are defined as x . In section 3.7 we have shown how to define an impact function, say, $\widehat{h}(x)$ by using the climate model and an AOT criterion. In order to couple the economic and the climate model, we consider the reduced order⁵ optimization problem

$$\max_{x \in \mathbb{R}^k} \{V(x) \mid \widehat{h}(x) \leq \Theta\}, \quad (28)$$

where Θ is a limit imposed on the impact. In what follows, to ease the notation, we use $h(x)$ instead of $\widehat{h}(x)$, with $h(x) := \widehat{h}(x) - \Theta$.

5.1 A cutting plane approach

$V(x)$ is concave by construction and for a cutting plane method to converge $h(x)$ must be convex⁶. Since the functions $V(x)$ and $h(x)$ are defined implicitly, we will construct a sequence of supporting planes to the epigraphs of $-V(x)$ and $h(x)$. These supporting planes are called cutting planes in the cutting plane framework.

In the cutting plane procedure we consider a sequence of points $\{x^n\}$ in the domain of $V(x)$. We denote Sv^n a subgradient of $V(x)$ at x^n , that is, $Sv^n \in \partial V(x^n)$, the subdifferential of $V(x)$ at x^n (given that $V(x)$ is concave, properly speaking we should talk about *antisubgradient* and *antisubdifferential*). If x^n is feasible, that is, $h(x^n) \leq 0$, we then define the linear approximation to $V(x)$ at x^n , given by $\widetilde{V}^n(x) = V(x^n) + Sv^n \cdot (x - x^n)$. If x^n is infeasible, that is, $h(x^n) > 0$, we define the linear approximation to $h(x)$ at x^n , $\widetilde{h}^n(x) = h(x^n) + Sh^n \cdot (x - x^n)$ and we introduce the auxiliary constraint $\widetilde{h}^n(x) \leq 0$.

In the cutting plane literature the point x^n is referred to as a *query point*, and the procedure to compute the objective value and subgradient at a query point is called an *oracle*. Furthermore, the hyperplane that approximates the objective function $V(x)$ at a feasible query point and defined by the equation $z = \widetilde{V}^n(x)$, is referred to as an *optimality cut*. The hyperplane that approximates the constraint function $h(x)$ at an infeasible query point and defined by the equation $\widetilde{h}^n(x) = 0$, is called a *feasibility cut*. See Fig. 1.

Let $\{x^n\}$, $n \in \mathcal{N} = \mathcal{N}_o \cup \mathcal{N}_f$ be a sequence of query points, where \mathcal{N}_o corresponds to the optimality cuts and $\mathcal{N}_f = \mathcal{N} \setminus \mathcal{N}_o$ to the feasibility cuts, respectively. A lower bound to the maximum value of $V(x)$ is provided by:

$$\theta_l = \max_{n \in \mathcal{N}_o} V(x^n).$$

The localization set is defined as

$$\mathcal{L}_{\mathcal{N}} = \{(x, z) \in \mathbb{R}^{k+1} \mid z \leq \widetilde{V}^n(x) \forall n \in \mathcal{N}_o, \quad z \geq \theta_l, \quad \widetilde{h}^n(x) \leq 0 \forall n \in \mathcal{N}_f, \quad x \in D\}, \quad (29)$$

⁵The problem is reduced to the coupling variables only.

⁶Indeed one cannot guarantee the convexity of $h(x)$ which is the result of a complex and highly non-linear numerical process. In practice, however, it is observed that the behaviour of $h(x)$ is close to convexity in the domain of interest for x . The nonconvexity of $h(x)$ may generate an empty localization set (a concept to be introduced shortly) during the cutting plane procedure. There are techniques permitting a backtracking in the procedure in order to overcome the local nonconvex behaviour (see [5])

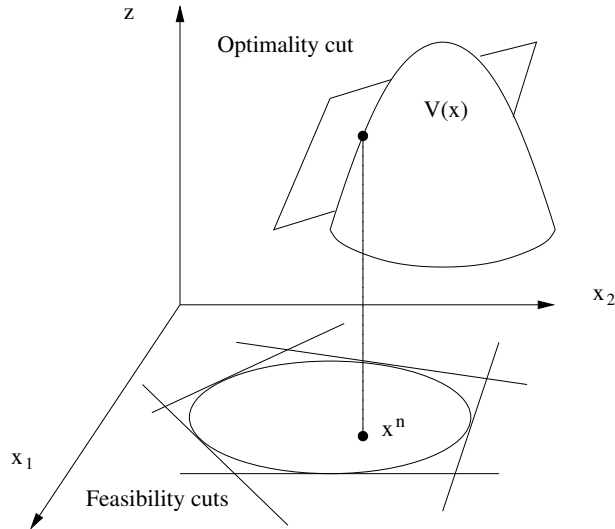


Figure 1: Optimality and feasibility cuts

where D is a compact domain defined for example by a set of lower and upper bounds for the components of x . The basic iteration of a cutting plane method can be summarized as follows

1. Select (\bar{z}, \bar{x}) in the localization set \mathcal{L}_N .
2. Call the oracle at \bar{x} . The oracle returns one or several cuts and, if all of them are optimality cuts, a new lower bound $V(\bar{x})$ is computed. Else, go to step 4.
3. Update the bounds:
 - (a) If \bar{x} is feasible, $\theta_l \leftarrow \max\{V(\bar{x}), \theta_l\}$.
 - (b) Compute an upper bound θ_u to the optimum⁷ of problem (28).
4. Update the lower bound θ_l in the definition of the localization set (29) and add the new cuts.

These steps are repeated until a point is found such that $\theta_u - \theta_l$ falls below a prescribed optimality tolerance. The reader may have noticed that the first step in the summary is not completely defined. Actually, cutting plane methods essentially differ in the way one chooses the query point. For instance, the intuitive choice of the Kelley point (\bar{z}, \bar{x}) that maximizes z in the localization set [20] may prove disastrous, because it over-emphasizes the global approximation property of the localization set. Safer methods introduce a regularizing scheme to avoid selecting points too “far away” from the best recorded point. The approach used in ACCPM (*Analytic Center Cutting Plane Method*) [12, 13, 28, 6] consists in selecting the *analytic center* of the localization set. Formally, the analytic center is the point (\bar{z}, \bar{x}) that minimizes the logarithmic barrier function⁸ of the localization set. If the set is bounded⁹ the analytic center is uniquely defined. Moreover the point is relatively easy to compute using the standard artillery of Interior Point Methods¹⁰. ACCPM easily handles both feasibility and optimality cuts. Furthermore, ACCPM is robust, efficient and particularly useful when the oracle is computationally costly —as is the case in this application.

⁷For example, $\theta_u = \max\{z \mid (z, x) \in \mathcal{L}_N\}$.

⁸The logarithmic barrier for the half space $\{x \mid a \cdot x \leq b\}$ is $-\log(b - a \cdot x)$.

⁹In practice, this assumption is met by setting appropriate, possibly very large, bounds on the variable x .

¹⁰ACCPM is pseudo-polynomial under mild assumptions.

The above basic iteration of the cutting plane method in the present case can be interpreted as follows

1. Select a vector of upper bounds on GHG concentrations, $x^n = (MA_1^{\text{sup}}, \dots, MA_k^{\text{sup}})'$ within the search region.
2. By using the C-GOLDSTEIN oracle, compute the associated AOTⁿ, that is, compute the value $h(x^n)$.
 - (a) If AOTⁿ is greater than the threshold Θ ($h(x^n) > \Theta$), AOTⁿ is not admissible and a feasibility cut ($\tilde{h}^n(x) \leq \Theta$) is generated at x^n . The role of this feasibility cut is to separate x^n from the search region D .
 - (b) Otherwise, AOTⁿ is admissible and an optimality cut is generated at x^n . The optimality cut is a linear approximation of $V(x)$ at x^n . Obviously, the optimal utility computed by the RCEG oracle, $V(x^n)$, is a lower bound to the optimal utility.
3. The set of feasibility cuts approximates the set of admissible bounds on GHG concentration. On the other hand, the set of optimality cuts approximates the function $V(x)$. Therefore, at each step 2 we generate either a feasibility cut or an optimality cut, which give an increasingly accurate piecewise affine approximation of the problem (28).

5.2 Implementation details

In this section we explain how to compute the subgradients Sv^n , Sh^n and a good starting query point x^0 . It can be seen that the set of optimal Lagrangian multipliers λ^n associated to constraints (26-27) when computing $V(x^n)$ gives a subgradient of $V(x)$ at x^n . That is, in the cutting plane procedure we set $Sv^n = \lambda^n$, where λ^n is obtained from the solution of RCEG. It is not so easy to compute $Sh^n = (Sh_1^n, \dots, Sh_k^n)'$, a subgradient of the climate function $h(x)$ at x^n . The only feasible way is to approximate its components by the finite differences:

$$Sh_i^n \simeq \frac{h(x^n + \epsilon e_i) - h(x^n)}{\epsilon}, \quad i = 1, \dots, k, \quad (30)$$

where $e_i = (0, \dots, 0, 1_i, 0, \dots, 0)'$ is the i -th canonical vector and $\epsilon > 0$.

To choose a good starting point, we notice that a no-emissions scenario gives a lower bound for the x values which correspond to the lowest possible carbon accumulation in the atmosphere. An RCEG scenario with no environmental constraints, also called a *Business As Usual* scenario, provides an upper bound for the x values. If we vary x at $t = 100$ and $t = 200$ years, that is, x_{10} and x_{20} , between these bounds, interpolate linearly to obtain $x(t)$ at other times, and compute the corresponding AOT values $\hat{h}(x)$ at a sparse, uniform grid of points in the enclosed rectangular region of $x_2 - x_4$ space, we obtain the graph shown in Figure 2. On this figure, regions with the same subgradient have the same colour. We observe that in the region of interest (an AOT greater than 10%) the response is almost linear. A linear regression gives an R^2 of 0.99 and the expression of $L_{\hat{h}}$:

$$L_{\hat{h}}(x_{10}, x_{20}) = 5.88 \cdot 10^{-4} x_{10} + 2.20 \cdot 10^{-3} x_{20} - 3.53 \quad (31)$$

The starting point for solving the full coupled problem using ACCPM has been selected by solving the following problem based on this linear approximation:

$$\max_{x \in \mathbb{R}^k} \{V(x) \mid L_{\hat{h}}(x_{10}, x_{20}) \leq \Theta\}. \quad (32)$$

The starting point thus obtained proves to be already quite close to the feasible region.

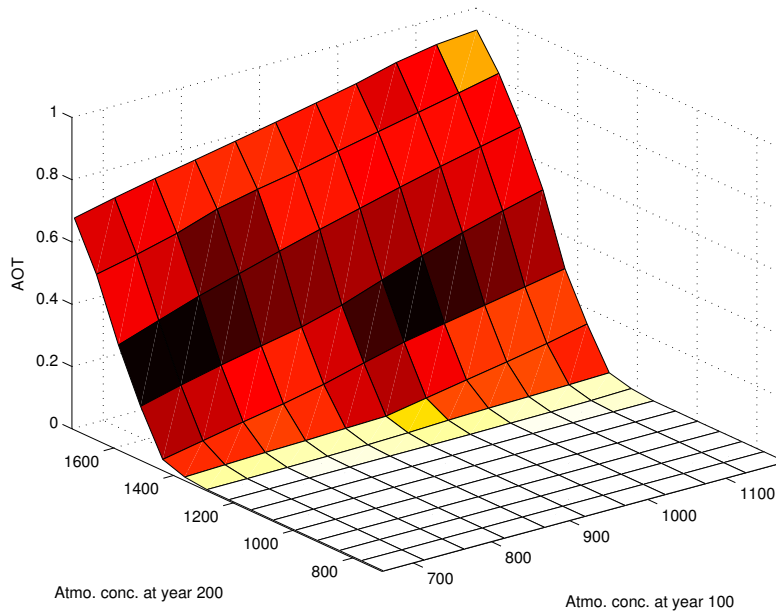


Figure 2: The impact $h(x)$ (AOT) from the climate model, as a function of only 2 variables, the concentrations at 100 and 200 years, with intermediate values defined linearly. This approximate form is used to define an initial condition.

6 Numerical results

6.1 Reference scenario from DICE99

Table 4: Output of an uncoupled run of DICE99 for years 1995-2085

Year	1995	2005	2015	2025	2035	2045	2055	2065	2075	2085
Output	22.563	30.068	37.486	44.985	52.644	60.492	68.54	76.792	85.258	93.948
Pccon	3	3.528	3.966	4.373	4.778	5.194	5.625	6.076	6.549	7.044
Savrate	0.2511	0.2392	0.2321	0.2277	0.2248	0.223	0.222	0.2215	0.2215	0.2217
Indem	59.1145	69.743	77.899	84.542	90.149	94.978	99.207	102.99	106.502	109.958
Sigma	0.272	0.2447	0.2232	0.2059	0.1916	0.1797	0.1695	0.1607	0.153	0.1461
Temp	0.43	0.502	0.613	0.749	0.901	1.063	1.23	1.4	1.573	1.749
Conc	735	775.63	818.03	860.73	903.27	945.44	987.07	1028	1068.26	1107.78
Ctax	8.15	11.17	14.38	17.85	21.61	25.64	29.89	34.25	38.58	42.61
Intrate	0.079	0.058	0.05	0.046	0.044	0.042	0.041	0.04	0.039	0.037
Discrate	1	0.7441	0.5578	0.4212	0.3202	0.2452	0.189	0.1466	0.11447	0.08993
Prod	0.017	0.018	0.019	0.02	0.021	0.022	0.023	0.025	0.026	0.027
Exogforc	-0.15	-0.165	-0.165	-0.149	-0.118	-0.072	-0.01	0.067	0.16	0.268
Pop	5632.7	6484.3	7258.3	7944.4	8540.3	9049.7	9479.5	9838.4	10135.6	10380.1
Etree	11.28	10.152	9.1368	8.2231	7.4008	6.6607	5.9947	5.3952	4.8557	4.3701
Margy	10005.2	6330.9	4221.3	2890.2	2011.5	1416.9	1008.3	724.14	524.588	383.166
Margc	10005.2	6330.9	4221.3	2890.2	2011.5	1416.9	1008.3	724.14	524.588	383.166
miu	0.038	0.053	0.07	0.089	0.109	0.129	0.15	0.17	0.19	0.206
Total emissions	70.394	79.894	87.036	92.765	97.549	101.64	105.2	108.39	111.358	114.328
Interest rate	0.0789	0.0584	0.0503	0.0464	0.0441	0.0424	0.041	0.0397	0.0385	0.0374
Damages	0.01697	0.029	0.0503	0.0849	0.1368	0.2102	0.3092	0.4382	0.6018	0.80521
Abatement cost	0.00087	0.002	0.004	0.0069	0.0111	0.0168	0.0244	0.0337	0.04468	0.05662

In Tables 4 and 5 we report the output of a run of the original, uncoupled DICE99 model, over a time horizon of 200 years. Of interest is the accumulation of GHG concentrations and the average temperature increase shown in Figures 3-4. According to DICE99, the economic growth generates an average temperature increase of 3.2 C over the 200 years. If we use the predicted atmospheric GHG concentrations to force C-GOLDSTEIN in a one-way coupling, with no feedback on DICE99, we obtain an average temperature increase of 2.6 C, while the

Table 5: Output of an uncoupled run of DICE99 for years 2095-2185

Year	2095	2105	2115	2125	2135	2145	2155	2165	2175	2185
Output	102.879	112.067	121.529	131.332	141.489	151.949	162.479	172.27	178.421	167.02
Pecon	7.562	8.105	8.673	9.271	9.905	10.59	11.37	12.393	14.23	14.138
Savrate	0.2223	0.223	0.2238	0.2247	0.225	0.2236	0.2165	0.1913	0.1006	0.0429
Indem	113.63	117.856	122.966	129.394	137.666	148.264	161.262	175.48	188.218	169.672
Sigma	0.1399	0.1343	0.1291	0.1242	0.1197	0.1153	0.111	0.1069	0.1029	0.0989
Temp	1.927	2.108	2.292	2.446	2.583	2.711	2.836	2.962	3.092	3.23
Conc	1146.76	1185.54	1224.68	1264.91	1307.2	1352.84	1403.32	1459.9	1522.58	1588.82
Ctax	46.03	48.4	49.31	48.23	44.48	37.45	26.97	14	0	UNDF
Intrate	0.036	0.035	0.034	0.033	0.033	0.032	0.032	0.033	0.039	0.075
Discrate	0.07108	0.05651	0.04519	0.03634	0.02939	0.02389	0.01952	0.016	0.01323	0.01098
Prod	0.029	0.03	0.031	0.033	0.034	0.036	0.038	0.039	0.041	0.043
Exogforc	0.392	0.53	0.53	0.53	0.53	0.53	0.53	0.53	0.53	0.53
Pop	10580.2	10743.3	10875.6	10982.8	11069.5	11139.3	11195.6	11241	11277.3	11306.5
Etree	3.9331	3.5398	3.1858	2.8672	2.5805	2.3225	2.0902	1.8812	1.6931	1.5238
Margy	282.092	209.267	156.386	117.647	89.036	67.698	51.526	38.826	27.909	23.299
Margc	282.092	209.267	156.386	117.647	89.036	67.698	51.526	38.826	27.909	23.299
miu	0.219	0.227	0.228	0.22	0.202	0.17	0.125	0.069	0	0
Total emissions	117.563	121.395	126.152	132.261	140.246	150.587	163.352	177.36	189.911	171.196
Interest rate	0.0363	0.0353	0.0343	0.0334	0.0326	0.0319	0.0316	0.0329	0.0391	0.0747
Damages	1.05427	1.35582	1.718	2.09594	2.49928	2.93703	3.41525	3.9271	4.40919	4.47555
Abatement cost	0.0683	0.07784	0.08317	0.08187	0.07187	0.05294	0.02894	0.0085	0	0

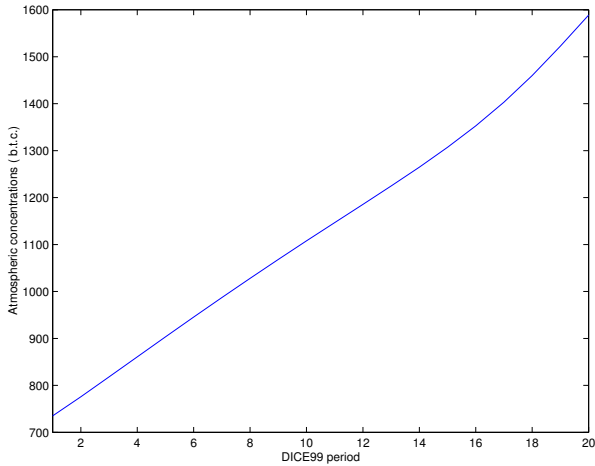


Figure 3: Atmospheric GHG concentration from an uncoupled run of DICE99.

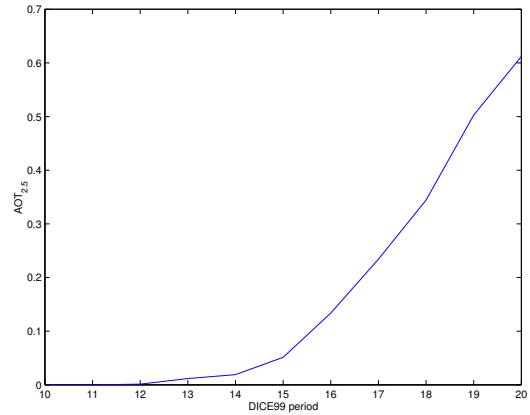


Figure 4: Global fraction where warming exceeds 2.5 C (AOT) between 2085 and 2185 from C-GOLDSTEIN forced by GHG concentrations from an uncoupled run of DICE99.

$AOT_{2.5}[200]$ takes a value of 0.612, *i.e.* C-GOLDSTEIN predicts more than 2.5 C warming, locally, for 61% of the globe at the year 2085, using the concentration path obtained from the DICE99 simulation.

6.2 RCEG with constraints on $AOT_{2.5}[200]$

In comparison with DICE99, the new control problem (11)-(27) defining the RCEG model no longer contains the equations which deal with temperature and forcing. The equation (18) was also modified as the production loss due to temperature impact is removed from the production function. We now run the model in a cost-effectiveness manner instead of the cost-benefit approach implemented by Nordhaus. For that purpose we introduce upper bounds on atmospheric concentrations (26)-(27) at milestones distributed 50 years apart (unless otherwise stated) along the time axis. The objective is to maximize the total welfare of the economic system subject to the concentration limits.

It is important to recall that these upper limits on concentrations will be obtained as a way to ensure that the constraint $AOT_{2.5}[200] \leq 0.5$ is satisfied. ACCPM is used to reach that optimum under constraint. Table 6 indicates the sequence of calls to the oracles and the query points. We observe that three feasibility cuts are introduced at the beginning and then an optimality cut is introduced to reach an optimal solution. The desired value $AOT_{2.5}[200] \leq 0.5$ is obtained after only 4 cuts.

Table 6: Calls of the oracles and query points in the ACCPM run

Milestones	50	100	150	200	Criterion	AOT	Type of cut
Starting point	= 918.26	1168.78	1422.76	1521.50	-	0.60917	Feasibility
Query point 1	= 916.57	1165.31	1416.16	1479.14	-	0.51365	Feasibility
Query point 2	= 915.99	1164.79	1415.38	1474.37	-	0.50193	Feasibility
Query point 3	= 915.63	1164.58	1415.14	1472.97	27506.02	0.49929	Optimality
End Point	= 915.20	1165.53	1414.60	1473.28	27504.74	0.49972	End

The same experiment is now repeated with a 19-dimensional coupling variable x (one component for each decade). The result is a smoother concentration path but, in this case, 24 cuts are required to reach a converged solution. Figure 5 shows the atmospheric concentration paths from the two experiments (denoted RCEG4 and RCEG20) along with the atmospheric concentration path from the uncoupled run of DICE99.

6.3 RCEG with constraints on various $AOT_{2.5}[200]$

In the last section, we observed an increase, then a decrease of the level of atmospheric concentrations for the two last decades. This reflects an unrealistic end-of-period effect where the economic system waits for the last moment to realize the abatement required. To reduce this effect, we modify the RCEG model slightly. We add a constraint that the growth of atmospheric GHG concentration is non-negative throughout the 200-year period;

$$MA(t-1) \leq MA(t) \tag{33}$$

Then the time horizon for the RCEG model is increased to 250 years but we still compute an AOT for year 200.

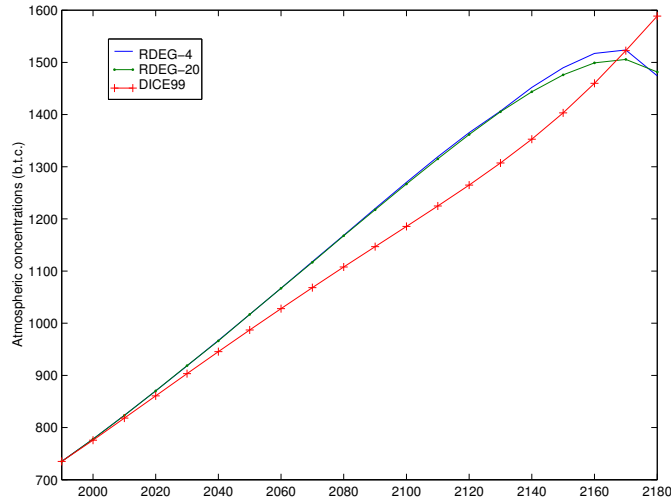


Figure 5: Atmospheric concentrations in b.t.c.

6.4 Target dependence on AOT threshold levels for RCEG

In Table 7 we report on the behavior of the CO_2 target values x as a function of AOT threshold value. Note that it is the threshold area which is changed. The temperature threshold remains fixed at 2.5 C local warming. We change the threshold for the control problem (11)-(27) and we allow the method to choose the optimal target values for different AOT values. We note that the target values for the early periods (50 and 100) remain essentially constant and the later periods (150 and 200) undergo a steady rise with increasing AOT threshold. This rise is attributed to an accumulation of CO_2 in later periods and the delayed adjustment of the economic system to regulations. The relatively smaller target values for reduced AOT thresholds for targets 150 and 200 (compared to targets 50 and 100) are consistent with the “end-of-period” effect described in the previous section.

Another observation is the behavior of the targets 150 and 200 for thresholds below 0.3. The 150 target has a larger value for low thresholds and this may be an indication of the importance of short-term target goals (150 years as opposed to 200 years) when temperatures bounds are more restrictive. Finally, the 150 year target shows a decline and approaches the 200 year target value for large values of AOT threshold. This behavior is expected in these very non-restrictive scenarios. Figure 6 shows the four target behaviors for varying AOT thresholds.

6.5 RCEG with constraints on weighted $AOT_{2.5}[200]$

The climate has different impacts on the economy depending on the region. We expect a more important impact on the northern continents and polar regions than the southern continents and therefore report an example experiment with the relative weights in these regions set to 2, 1.5 and 1 respectively. Ocean regions have zero weight in this experiment. The computation of the weighted AOT is given by equation (10). Figure 7 shows the comparison between the weighted and unweighted AOT runs. Differences are small initially, but the weighted AOT is slightly more restrictive owing to enhanced heating over northern continents.

Table 7: Results of the change in AOT threshold for C-GOLDSTEIN model

AOT _{2.5} [200]	Milestone targets			
	50	100	150	200
0.1	916.12	1151.63	1390.15	1326.39
0.2	917.92	1156.73	1396.21	1369.66
0.3	917.51	1162.32	1369.31	1417.52
0.4	917.78	1166.41	1401.64	1450.25
0.5	918.26	1166.02	1415.96	1486.76
0.6	917.42	1169.13	1422.66	1525.24
0.7	918.22	1170.02	1423.66	1575.77
0.8	918.41	1173.55	1436.73	1638.92
0.9	918.24	1172.02	1427.24	1600.89
1.0	918.17	1168.72	1422.76	1580.72

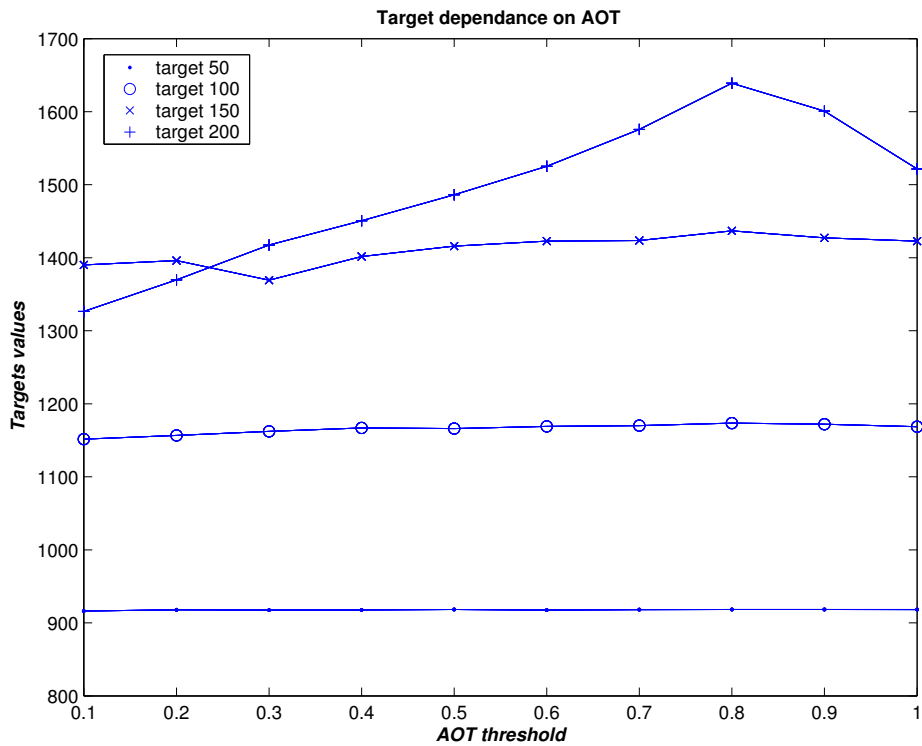


Figure 6: Target CO2 dependence on AOT threshold levels

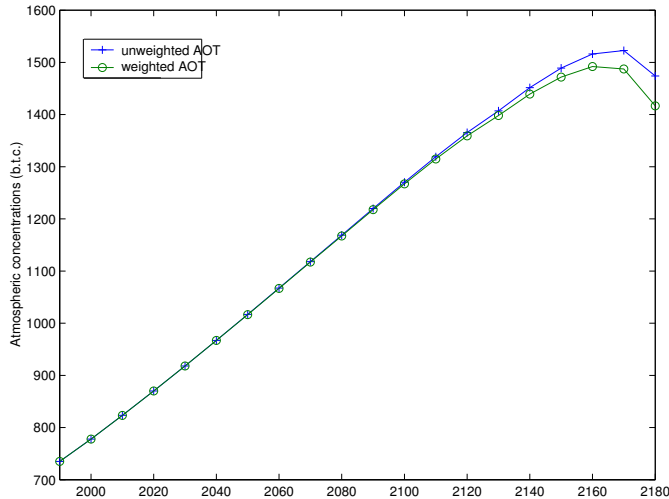


Figure 7: Atmospheric concentrations obtained by constraining the regionally weighted AOT to be less than 50%

7 Conclusion

In this paper, we have shown how modern convex optimization techniques can be harnessed to couple an economic model and a climate model characterized by different time and space scales. The coupling variables are the GHG concentrations as a function of time, and a set of impact criteria calculated by the climate model. We have solved a reduced-order problem in which the concentrations are assumed to vary linearly between 4 variable “targets” at 50-year intervals. The optimal solution is located by reducing the volume of the solution domain iteratively using a sequence of cutting planes. A very efficient choice of these planes gives a quick convergence towards the solution. ACCPM fulfills this task. Here the climate model, C-GOLDSTEIN, calculates a single impact criterion, the area of the globe where the surface warming exceeds a given threshold, an “Area Over Threshold” criterion. We have also weighted the “area” by region to represent a more realistic impact on the global economy. In general, the response of the economic model, RCEG, when a given constraint is enforced on the AOT, is a loss of production.

Allowing the two models to interact fully results in changes to the optimal emissions scenarios calculated by the economic model. In this initial test, our use of an impact criterion which depends only on the final state can result in unrealistic end effects. This problem could be addressed by including further impact criteria with more general time dependence such as a maximum rate of warming.

A remaining inconsistency is that the economic model uses a simplified representation of carbon transfer to the ocean. However, the simple experiments we have performed here are sufficient to demonstrate the feasibility and efficiency of our approach. The important feature of the coupling described here is that our technique allows us to maintain the full complexity of each of the submodels. In future, we plan to build on this work by replacing RCEG with a more complex economic model. A modified version of the ICLIPS model would introduce a regional scale for the economy, whereas the MERGE model would add a regional scale and energy response to climate change. To make the coupling completely consistent, the recycling of atmospheric carbon should be calculated by the climate component, for instance by using versions of the GENIE model. With a more comprehensive integrated meta-model, it would become appropriate to study the coupling in more detail and experiment with further constraints,

for example changes in Atlantic overturning and changes in precipitation as well as temperature. A further interesting possibility would be to include a simplified representation of the feedback effects of changes in land use.

References

- [1] LEIMBACH M., TOTH F. L.. (2003) *Economic Development and Emission Control over the Long Term: The ICLIPS Aggregated Economic Model*, Special Issue of **Climatic Change** on the ICLIPS Project: Vol. 56, No. 1-2, 2003.
- [2] ALCAMO, J. (Ed. 1994) *IMAGE 2.0: Integrated Modelling of Global Climate Change.*, Kluwer, London.
- [3] BAHN, O., EDWARDS, N.R., KNUTTI, R. AND STOCKER, T.F. *E-MERGE, first evaluations of mitigation policies preserving the Atlantic thermohaline circulation.* (in preparation)
- [4] BOVILLE BA, GENT PR (1998) *The NCAR climate system model, version one.* **J Clim** 11: 1115-1130
- [5] CARLSON D.A., A. HAURIE, J.-P. VIAL AND D. S. ZACHARY, *Large Scale Convex Optimization Methods for Air Quality Policy Assessment*, to appear **automatica**, 2004.
- [6] DU MERLE O. AND J.-P. VIAL (2002) *Proximal accpm, a cutting plane method for column generation and lagrangian relaxation: application to the p-median problem.* Technical report, Logilab, HEC, University of Geneva.
- [7] EDWARDS NR (1996) *Unsteady similarity solutions and oscillating ocean gyres.* **J Marine Res** 54: 793-826
- [8] EDWARDS NR AND MARSH R., *Uncertainties due to transport-parameter sensitivity in an efficient 3-D ocean-climate model*, submitted to **Climate Dynamics**.
- [9] EDWARDS NR, WILLMOTT AJ, KILLWORTH PD (1998) *On the role of topography and wind stress on the stability of the thermohaline circulation.* **J Phys Oceanogr** 28: 756-778
- [10] EDWARDS NR, SHEPHERD JG (2002) *Bifurcations of the thermohaline circulation in a simplified three-dimensional model of the world ocean and the effects of interbasin connectivity.* **Climate Dynamics** 19: 31-42
- [11] <http://www.genie.ac.uk>
- [12] GOFFIN J.-L., HAURIE A. AND VIAL J.-P. (1992) *Decomposition and non-differentiable optimization with the projective algorithm*, **Management Science** 38: 284-302
- [13] GOFFIN J.-L. AND J.PH. VIAL (1999) *Convex nondifferentiable optimization: a survey focussed on the analytic center cutting plane method.* Technical Report 99.02, Geneva University - HEC - Logilab, February.
- [14] GOOSSE H, SELTEN FM, HAARSMA RJ, OPSTEEGH JD (2001) *Decadal variability in high northern latitudes as simulated by an intermediate-complexity climate model.* **Annals of Glaciology** 33: 525-532
- [15] GORDON C, COOPER C, SENIOR CA, BANKS H, GREGORY JM, JOHNS TC, MITCHELL JFB, WOOD RA (2000) *The simulation of SST, sea-ice extents and ocean heat transports in a version of the Hadley Centre coupled model without flux adjustments.* **Climate Dynamics** 16: 147-168

- [16] GRIFFIES SM (1998) *The Gent-McWilliams skew flux*. **J Phys Oceanogr** 28: 831-841
- [17] HIBLER WD (1979) *A dynamic thermodynamic sea ice model*. **J Phys Oceanogr** 9: 815-846
- [18] JAEGER C., LEIMBACH M., CARRARO C., HASSELMANN K., HOURCADE J.C., KEELER A., KLEIN R., *Community integrated assessment: Modules for cooperation*, FEEM Nota di Lavoro, 2002.
- [19] JOSEY SA, KENT EC, TAYLOR PK (1998) *The Southampton Oceanography Centre (SOC) Ocean-Atmosphere Heat, Momentum and Freshwater Flux Atlas*. Southampton Oceanography Centre Rep. 6, Southampton, United Kingdom, 30 pp. + figures
- [20] KELLEY J. E. (1960) *The cutting-plane method for solving convex programs*. **Journal of the SIAM**, 8:703-712.
- [21] KILLWORTH PD (2003) *Some physical and numerical details of frictional geostrophic models*. Southampton Oceanography Centre internal report 90
- [22] MANN A.S., R. MENDELSON AND R.G. RISHELS (1995) *MERGE: A model for evaluating regional and global effects of GHG reduction policies* **Energy Policy** 23: 17-34
- [23] MARSH R, YOOL A, LENTON TM, GULAMALI MY, EDWARDS NR, SHEPHERD JG () *Bistability of the thermohaline circulation identified through comprehensive 2-parameter sweeps of an efficient climate model*. Submitted to **Climate Dynamics**
- [24] NORDHAUS W.D. (1992) *An optimal transition path for controlling greenhouse gases*. **Science** 258: 1315-1319
- [25] NORDHAUS W.D. (1994) *Managing the Global Commons: The Economics of Climate Change*, MIT Press, Cambridge, Mass.
- [26] NORDHAUS W.D. AND J. BOYER (2000) *Warming the World: Economic Models of Global Warming*, MIT Press, Cambridge, Mass.
- [27] OORT AH (1983) *Global atmospheric circulation statistics, 1958-1973*: NOAA Prof Pap 14
- [28] PETON O. AND J.-P. VIAL (2001) *A brief tutorial on ACCPM*. Technical report, Logilab, HEC, University of Geneva.
- [29] RAMSEY F. (1928) *A mathematic theory of saving*, **Economic Journal** 38r: 543-549
- [30] SEMTNER AJ (1976) *A model for the thermodynamic growth of sea ice in numerical investigations of climate*. **J Phys Oceanogr** 6: 379-389
- [31] SINHA B, SMITH RS (2002) *Development of a fast Coupled General Circulation Model (FORTE) for climate studies, implemented using the OASIS coupler*. Southampton Oceanography Centre Internal Document, No. 81: 67pp
- [32] SHEPHERD JG (2003) *Overcoming the CFL time-step limitation: a stable iterative implicit numerical scheme for slowly evolving advection-diffusion systems*. **Ocean Modelling**, Submitted
- [33] THOMPSON SJ, WARREN SG (1982) *Parameterization of outgoing infrared radiation derived from detailed radiative calculations*. **J Atmos Sci** 39: 2667-2680

- [34] WEAVER AJ, EBY M, WIEBE EC, BITZ CM, DUFFY PB, EWEN TL, FANNING AF, HOLLAND MM, MACFADYEN A, MATTHEWS HD, MEISSNER KJ, SAENKO O, SCHMITTNER A, WANG H, YOSHIMORI M (2001) *The UVic Earth System Climate Model: Model description, climatology, and applications to past, present and future climates*. **Atmos-Ocean** 39: 361-428
- [35] WRIGHT DG, STOCKER TF (1991) *A zonally averaged ocean model for the thermohaline circulation. Part I: Model development and flow dynamics*. **J Phys Oceanogr** 21: 1713-1724
- [36] ZAUCKER F, BROECKER WS (1992) *The influence of atmospheric moisture transport on the fresh water balance of the Atlantic drainage basin: General Circulation Model simulations and observations*. **J Geophys Res** 97: 2765-2773

Working Papers of the WP Climate Risks Assessment

- WP4-1 Thalmann P. (2001). **The public acceptance of green taxes: 2 million voters express their opinion**, November.
- WP4-2 Haurie A. (2001). **Integrated assessment modeling for climate change: an infinite horizon optimization viewpoint** (Draft), December.
- WP4-3 Barrieu P., Chesney M. (2001), **Optimal timing for an environmental policy in a strategic framework**, October 16.
- WP4-4 Haurie A., Siverguina I., Zachary D. S. (2002), **A reduced-Order Photo-Chemical Air Quality Model**, January 23.
- WP4-5 Carlson D.A., Haurie A., Vial J.-P., Zachary D. S. (2002). **An Oracle Method for Coupling an E3 Model With a Photo-Chemical Air Quality Model**, January 30.
- WP4-6 Viguiet L. (2002). **The U.S. Climate Change Policy: A Preliminary Evaluation**, February 28.
- WP4-7 Chiera B., Filar J., Zachary D.S.(2002). **Comparative Forecasting Analysis of the ENSO**, June 19.
- WP4-8 Greppin H., Priceputu A. (2002). **Dialectique du bioespace et de l'écoespace : émergence de la territorialité, de la biocénose aux sociétés**, July.
- WP4-9 Bahn O., Kypreos S. (2002). **MERGE-ETL: An optimisation equilibrium model with two different endogenous technological learning formulations**, July.
- WP4-10 Haurie A. (2002). **Turnpikes in multi-discount rate environments and GCC policy evaluation**, August.
- WP4-11 Bernard A., Haurie A., Vielle M., Viguiet L. (2002). **A Two-Level Dynamic Game of Carbon Emissions Trading Between Russia, China, and Annex B Countries**, September.
- WP4-12 Greppin H., Degli Agosti R., Priceputu A. M. (2002). **From Viability Envelopes to Sustainable Societies**, October.
- WP4-13 Greppin H., Degli Agosti R., Priceputu A. M. (2002). **The Concept of Viability Envelopes**, November.
- WP4-14 Babiker M., Reilly J., Viguiet L. (2002). **Is Emissions Trading Always Beneficial?**, November.
- WP4-15 Haurie A., Viguiet L. (2002). **A Stochastic Dynamic Game of Carbon Emissions Trading**, December.
- WP4-16 Haurie A. (2003). **A Stochastic Multi-Generation Game with Application to Global Climate Change Economic Impact Assessment**, January.
- WP4-17 Viguiet L. (2003). **Defining meaningful participation of developing countries in climate change mitigation**, March.
- WP4-18 Haurie A. (2003). **A Multigenerational Game Model to Analyze Sustainable Development**, February.
- WP4-19 Bernard A., Paltsev S., Reilly J.M., Vielle M. & Viguiet L., 2003. **Russia's Role in the Kyoto Protocol**, MIT Joint Program on the Science and Policy of Global Change, Report 98, Cambridge, MA, June.
- WP4-20 Greppin H. Degli Agosti R., Priceputu A. (2003). **Utilisation de variables sentinelles de viabilité pour suivre l'évolution globale et locale du développement durable**, October.
- WP4-21 Bernard A., Vielle M., Viguiet L. (2003). **Carbon Tax and International Emissions Trading: A Swiss Perspective**, October.
- WP4-22 Viguiet L., Vielle M., Haurie A., Bernard A. (2003). **A Two-level Computable Equilibrium Model to Assess the Strategic Allocation of Emission Allowances Within the European Union**, October.
- WP4-23 Perret S. (2003). **La taxe CO2 en Suisse. Développements récents**, Octobre.
- WP4-24 Perret S. (2003). **La politique Suisse de réduction des émissions de gaz synthétiques**, Octobre.
- WP4-25 Perret S. (2003). **L'acceptabilité des instruments économiques dans le domaine de la politique climatique en Suisse: Résultats préliminaires**, Octobre.